ChemComm

Accepted Manuscript

This article can be cited before page numbers have been issued, to do this please use: X. Li, Y. Tang, J. Li, X. Hu, C. Yin, Z. Yang, Q. Wang, Z. Wu, X. Lu, W. Wang, W. Huang and Q. Fan, *Chem. Commun.*, 2019, DOI: 10.1039/C9CC02224D.




ROYAL SOCIETY OF CHEMISTRY

rsc.li/chemcomm

ROYAL SOCIETY OF CHEMISTRY View Article Online
DOI: 10.1039/C9CC02224D

Journal Name

COMMUNICATION

# A small-molecule probe for ratiometric photoacoustic imaging of hydrogen sulfide in living mice

Received 00th January 20xx,
Accepted 00th January 20xx

DOI: 10.1039/x0xx00000x

www.rsc.org/

Xiang Li,[a] Yufu Tang,[a] Jie Li,[a] Xiaoming Hu,[a] Chao Yin,[a] Zhen Yang,[a] Qi Wang,[a] Zizi Wu,[b] Xiaomei Lu,*[b] Wenjun Wang, Wei Huang [ab] and Quli Fan*[a]

**A small-molecule photoacoustic probe based on cyanine dyes was developed by taking advantage of the nucleophilic substitution reaction of $H_2S$ with chlorine. The probe demonstrated specific response to $H_2S$ with ratiometric photoacoustic signals in the NIR region, which enabled real-time, accurate, high-resolution imaging of endogenous $H_2S$ in vivo.**

In the last few decades, hydrogen sulfide ($H_2S$) has been recognized as a vital gaseous signaling molecule in living organisms. Biologically relevant $H_2S$ is enzymatically generated at micromolar levels from cysteine (Cys).[1] $H_2S$ exerts multifaceted regulatory functions in living systems, such as maintaining redox homeostasis, modulating neurotransmission, and stimulating vasodilation.[2] Abnormal $H_2S$ production is believed to be closely associated with diseases, such as Parkinson's disease, Down syndrome, and diabetes.[3] Such features make $H_2S$ a potential target for real-time imaging of pathological and physiological conditions in the living body.[1b] To date, various $H_2S$ responsive probes have been developed based on different trigger mechanisms, including reduction of azido or hydroxyamino,[5] reaction with electrophilic moieties,[5] and bonding to Cu(II) ion.[6] Among them, ratiometric probes are promising for reliable *in vivo* imaging because of the built-in self-calibration system, which can eliminate interference from the internal environment, such as heterogeneous probe biodistribution and excitation intensity.[7] However, these probes are primarily based on fluorescence imaging modality and have short tissue penetration depth and strong photon scattering, which limit precise measurement of $H_2S$ in deep tissues. Thus, ratiometric probes with new imaging modality should be developed for accurate detection of $H_2S$ in the living body.

An effective approach to address the aforementioned issues is photoacoustic (PA) imaging, which converts optical excitation into ultrasonic signal and avoids the influence of optical scattering in principle.[8] PA inherits the advantages of optical imaging, such as high sensitivity and non-invasiveness, and provides deep tissue penetration and excellent spatial resolution.[9] Given these extraordinary properties, ratiometric PA probes with NIR excitation have been successfully developed for accurate and high-resolution *in vivo* imaging of biological targets, including reactive oxygen (ROS),[10] metal ions,[11] Glutathione (GSH),[12] and pH.[13] However, the development of ratiometric PA probes for $H_2S$ remains a huge challenge because the ratio signal of two NIR absorption bands is difficult to construct at the molecular level. At present, most ratiometric PA probes are made of nanocomposites that integrate two different contrast agents to set an internal standard. Such multi-component systems experience leakage, which significantly affects the stability of the ratio signal. Moreover, most PA probes reported are highly hydrophobic and require to be encapsulated with biocompatible polymers. The increased size of the probes largely retains them in the reticuloendothelial system. FDA-approved NIR contrast agents, namely, methylene blue and indocyanine green (ICG), are small molecules that can be rapidly excreted. Thence, these probes are unsuitable for clinical application due to their potential long-term toxicity. Therefore, the development of small-molecule PA probes with ratiometric $H_2S$ response capability is of great significance for accurate monitoring of $H_2S$ *in vivo* and clinical translation of PA imaging.

In this study, we developed an ICG-like cyanine dye as ratiometric PA probe for real-time imaging of $H_2S$ in living mice (Scheme 1a). A ratiometric response strategy was constructed within a single small molecule based on the nucleophilic substitution of $H_2S$ with chlorine. Nucleophilic aromatic substitution ($S_NAr$) of electron-deficient aryl halides is

[a] *Key Laboratory for Organic Electronics and Information Displays & Jiangsu Key Laboratory for Biosensors, Institute of Advanced Materials (IAM), Jiangsu National Synergetic Innovation Center for Advanced Materials (SICAM), Nanjing University of Posts & Telecommunications, Nanjing 210023, China. E-mail: iamqlfan@njupt.edu.cn*
[b] *Key Laboratory of Flexible Electronics & Institute of Advanced Materials, Jiangsu National Synergetic Innovation Center for Advanced Materials, Nanjing Tech University (NanjingTech), Nanjing 211816, China*
[c] *Key Lab of Optical Communication Science and Technology of Shandong Province & School of Physics Science and Information Engineering, Liaocheng University, Liaocheng 252059, China*

† Electronic Supplementary Information (ESI) available: Experimental details, NMR spectra *etc*. See DOI: 10.1039/x0xx00000x

Q.F. and X.L. supervised and conceived the research; X.L. performed experiments; others analyzed the data and wrote the manuscript. All animal experiments were carried out in accordance with the guidelines of the Laboratory Animal Center of Jiangsu KeyGEN Biotech Corp., Ltd.

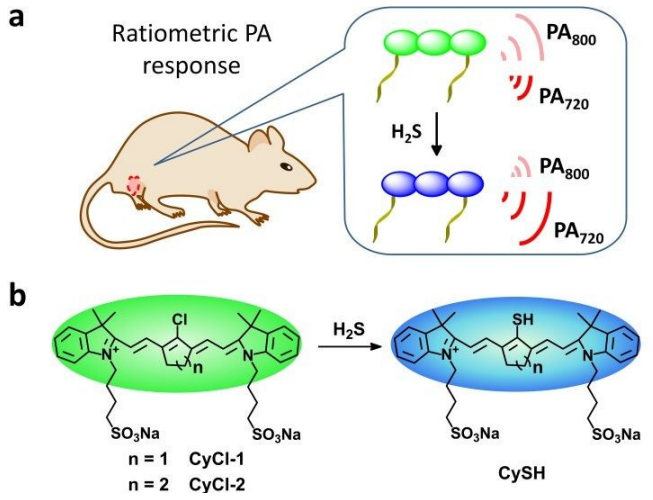


**Scheme 1** (a) The illustration of ratiomtetric PA detection of $H_2S$ *in vivo* with CyCl-1; (b) Structures of CyCl-1 or CyCl-2 and the proposed mechanism for $H_2S$ detection.

proven to be an efficient $H_2S$ detection strategy.[7a, 14] Cyanine dyes with active chlorine show strong electron deficiency due to the indolium group, and it should react with $H_2S$ under physiological conditions. In this regard, two chlorinated cyanine dyes, namely, CyCl-1 and CyCl-2 (Scheme 1b), were synthesized for $H_2S$ response studies. We envisioned that the substitution of $H_2S$ versus chlorine of the probes would shift their maximum absorption, which could provide a ratiometric PA signal for accurate detection of $H_2S$ *in vivo*.

CyCl-1 and CyCl-2 were synthesized from cyclopentanone and cyclohexanone to obtain different cycloolefin conjugated centers. Two sulfonate-terminated butyl chains were introduced to provide excellent aqueous solubility. The $^1$H NMR spectra of the two probes were similar due to their structural similarity. In CyCl-1, the peak of -$CH_2$- adjacent to the olefinic bonds presented as a singlet at 3.03 ppm (Figure S3) because the protons of two -$CH_2$- in the cyclopentenyl group are magnetically equivalent. While, in CyCl-2, the coupling effect from the additional -$CH_2$- in the cyclohexenyl group led to a triplet at 2.89 ppm (Figure S4). The mass spectrometry analysis revealed the maximum mass peaks of CyCl-1 and CyCl-2 at m/z 756.892 and 770. 936 (Figure S5), respectively, which are ascribed to $[M]^+$ species. These data indicated the successful synthesis of the probes. The analysis of the photophysical properties revealed a shift of 25 nm between the maximum absorption peaks of the two probes. CyCl-1 exhibited a maximum absorption peak at 800 nm and a shoulder peak at 725 nm, whereas CyCl-2 showed the maximum absorption peak at 775 nm and shoulder peak at 715 nm. In addition, CyCl-1 displayed higher absorbance than CyCl-2 (Figure S6). These conditions were probably due to the better coplanarity of the penta-cyclic than the hexa-cyclic structure.

The response of the probes to $H_2S$ was first investigated by absorption spectroscopy in phosphate- buffered saline (PBS, pH 7.4). The two probes were treated with 80 μM NaHS. The maximum absorption of CyCl-1 at 800 nm gradually decreased accompanied by the continuous enhancement of the shoulder peak. Finally, the maximum absorption peak shifted to 720 nm (Figure S7). After 10 min of incubation, the ratio of absorption intensity at 720 nm to 800 nm ($A_{720}/A_{800}$) showed an enhancement of 122.5-fold. Similar change in the absorption band was observed for CyCl-2 with a small degree of shift from 775 nm to 710 nm. However, the absorption intensity ratio of CyCl-2 ($A_{710}/A_{775}$) only enhanced by 10.2-fold (Figure 1a). The evolution of the absorption spectra could be attributed to the intramolecular charge transfer (ICT) of the probes before and after the substitution of chlorine with electron-donating $HS^-$,[15] which caused a visible color change in the probe solutions from green to blue (Figure S8). The response mechanism was confirmed through mass spectrometry characterization. After reaction with excess NaHS, new mass peaks at 776.909 and 791.015 were observed for CyCl-1 and CyCl-2, respectively, which are ascribed to the $[CySH-H+Na]^+$ species (Figure S9). These results indicated that $H_2S$ can replace the active chlorine of the probes through nucleophilic substitution under physiological conditions and lead to ratio changes in the absorption spectra in the NIR region.

Then, we quantitatively investigated the response kinetics and sensitivity of CyCl-1 and CyCl-2. The logarithmic value of

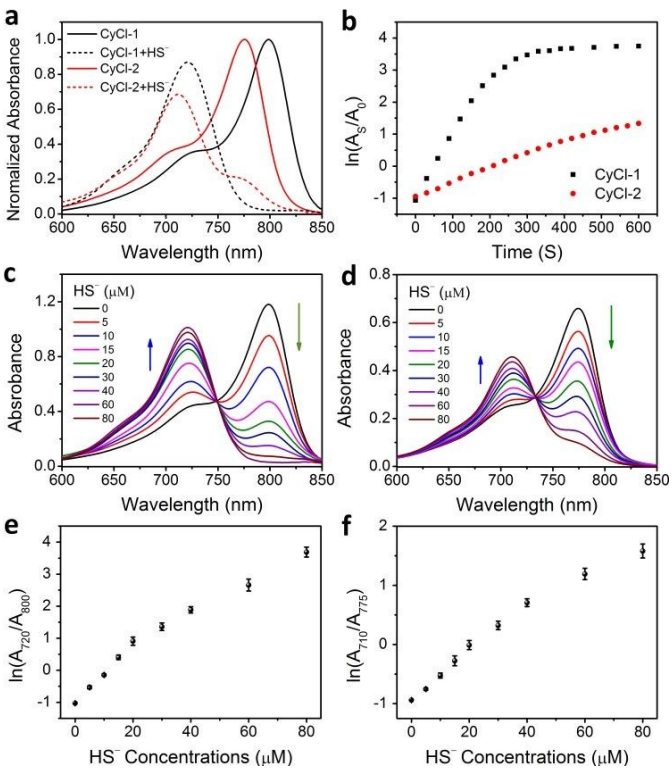


**Fig. 1** Normalized absorption of CyCl-1 and CyCl-2 (10 μM) before and after incubation with NaHS (80 μM) for 10 min in PBS buffer (pH 7.4); (b) The logarithmic value of the absorption intensity ratios [$\ln(A_{720}/A_{800})$ for CyCl-1 and $\ln(A_{710}/A_{775})$ for CyCl-2] of the probes as a function of incubation time; Absorption spectra evolution of CyCl-1 (c) and CyCl-2 (b) upon the addition of different concentrations of $HS^-$ from 0 to 80μM; The logarithmic value of the absorption intensity ratios of CyCl-1 (e) and CyCl-2 (f) as a function of $HS^-$ concentration.

the absorption intensity ratio [ln($A_{720}/A_{800}$) for CyCl-1 or ln($A_{710}/A_{775}$) for CyCl-2] was quantified as a function of reaction time after treatment with 80 μM NaHS (Figure 1b). The ratiometric signal of CyCl-1 [ln($A_{720}/A_{800}$)] increased rapidly after treatment with $HS^-$ and reached the equilibrium within 5 min. In comparison, the ratiometric signal of CyCl-2 [ln($A_{710}/A_{775}$)] showed slight increase even after 10 min of incubation. The absorption spectra of the probes showed gradual evolution over the $HS^-$ concentrations (Figures 1c and d), which permitted the quantitative detection of $H_2S$ through ratiometric absorption. The logarithmic value of the absorption intensity ratios increased linearly with $HS^-$ concentrations for the two probes (Figures 1e and f). The detection limits for $H_2S$ with CyCl-1 and CyCl-2 were determined to be 0.16 and 0.37 μM, respectively (Figure S10). These results indicated that CyCl-1 possessed faster response kinetics and higher sensitivity. In view of the strong NIR absorption and excellent responsiveness, CyCl-1 was selected as the PA probe for $H_2S$ imaging.

The PA response of CyCl-1 to $H_2S$ was first evaluated in the solution. The PA spectrum of CyCl-1 showed a maximum peak at 800 nm and a shoulder peak at 730 nm in PBS (pH 7.4). In the presence of $HS^-$, the PA peak at 800 nm almost disappeared, and the maximum peak shifted to 720 nm (Figure 2a). The change in the PA spectrum was similar to the absorption data, verifying the feasibility of CyCl-1 for ratiometric PA detection of $H_2S$. PA imaging of $H_2S$ in the solution with CyCl-1 was conducted through excitation at 720 and 800 nm, which were rendered with pseudo-colors of green and red, respectively (Figure 2b). With increasing $HS^-$ concentration, the PA signal at 720 nm continuously increased accompanied by a gradual attenuation of the PA signal at 800 nm. The limit of detection was caculated as 0.87 μM by using the logarithmic value of the PA intensity ratio [ln($PA_{720}/PA_{800}$)] as the detection signal (Figures 2c and S11). Hence, the probe can be used for PA detection of $H_2S$ under physiologically relevant concentrations.

We then evaluated the PA response selectivity of the probe toward $H_2S$. Compared with the significant enhancement of ratiometric PA signal ($PA_{720}/PA_{800}$) triggered by $H_2S$, other analytes, such as metal cations, ROS, reactive nitrogen and sulfur species, only induced negligible floating (Figure 2d). Competition assays were conducted with biothiols such as GSH and Cys. CyCl-1 exhibited potent response to NaHS in the presence of excess Cys (1 mM) or GSH (5 mM) (Figure S12), indicating the high response specificity to $H_2S$ over Cys and GSH. This condition could be ascribed to the stronger nucleophilicity of $H_2S$ than thiols.[16] CyCl-1 exhibited stable responsiveness to $H_2S$ within the biological pH range of 5.0 to 9.0 (Figure S13). Moreover, no obvious changes in the maximum absorption of the probe were observed after incubated in PBS containing 10% fetal bovine serum for 36 h (Figure S14), reflecting the good stability of the probe in blood. These data indicated the huge potential of the probe for $H_2S$ detection with minimized interference in biological systems. Furthermore, MTT assay revealed high cell viabilities under test concentrations of CyCl-1. The low cytotoxicity of the probe facilitated its application for PA imaging *in vivo*.

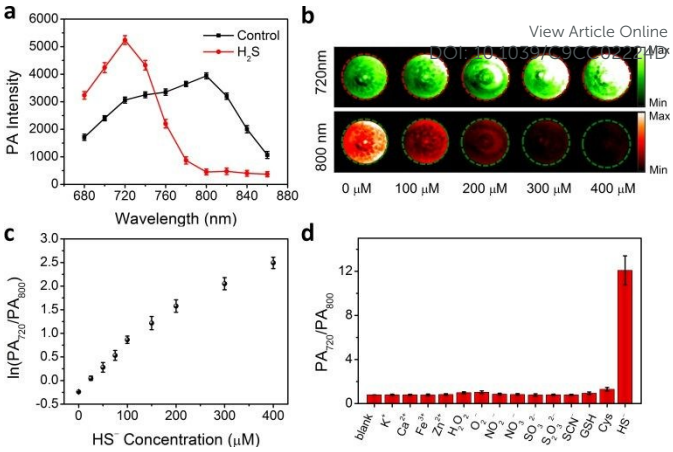


**Fig. 2** (a) PA spectra of CyCl-1 (50 μM) in PBS (pH 7.4) before (black line) and after (red line) incubation with 400 μM of $HS^-$; (b) PA images of CyCl-1 solution in the presence of different concentrations of $HS^-$, excitation at 800 nm (red) and 720 nm (green); (c) The logarithmic value of $PA_{720}/PA_{800}$ as a function of $HS^-$ concentration. (d) Ratiometric PA signals of CyCl-1 in the presence of $HS^-$ and other biological analytes.

The *in vivo* PA imaging of $H_2S$ with CyCl-1 was investigated in a mouse model. NaHS or PBS was subcutaneously injected into the thigh of living mice. The mice were then injected with CyCl-1 (50 μM, 10 μL) at the same locations, and the PA signals of the probe were recorded under excitation at 720 nm (green) and 800 nm (red). Figure 3 shows the PA images of the probe-treated regions. The boundary of the injection areas could be clearly demonstrated in these images, reflecting the excellent spatial resolution of PA imaging. The PA signal detected before injection of the probe was derived from the NIR absorption of hemoglobin in the blood. In order to minimize the background interference, the PA intensity increment (ΔPA), defined as the PA intensity after injection of CyCl-1 minus the PA intensity in the treated area before injection, was used to analyze the images. The PA increment at 720 ($\Delta PA_{720}$) and 800 nm ($\Delta PA_{800}$) for PBS treated mice significantly increased after injection of CyCl-1 and showed negligible variations over time (Figure 3a). While $\Delta PA_{800}$ increased less than $\Delta PA_{720}$ for NaHS treated mice after injection of CyCl-1 and showed opposite changes over time (Figure 3b), which suggested the activation of the probe by $HS^-$. The probe was further used to detect endogenous $H_2S$ in living mice. The mice were pretreated with Cys (precursor of $H_2S$) for 30 min, then CyCl-1 was injected. $\Delta PA_{720}$ and $\Delta PA_{800}$ showed the same variation trend as the mice treated with NaHS, after injection of CyCl-1 (Figure 3c). The quantitative analysis revealed that ln($\Delta PA_{720}/\Delta PA_{800}$) increased over time and reached 1.86 ± 0.12 and 0.93 ± 0.07 at 30 min for the mice treated with NaHS and Cys, respectively, which are higher than those in the control group (− 0.119 ± 0.04, Figure 3d). This result demonstrated the capability of CyCl-1 for real-time monitoring of endogenous $H_2S$ *in vivo* with ratiometric PA imaging. Furthermore, the pharmacokinetics studies revealed that CyCl-1 mainly accumulated in the liver after systemic administration (Figure S16a). Fluorescence

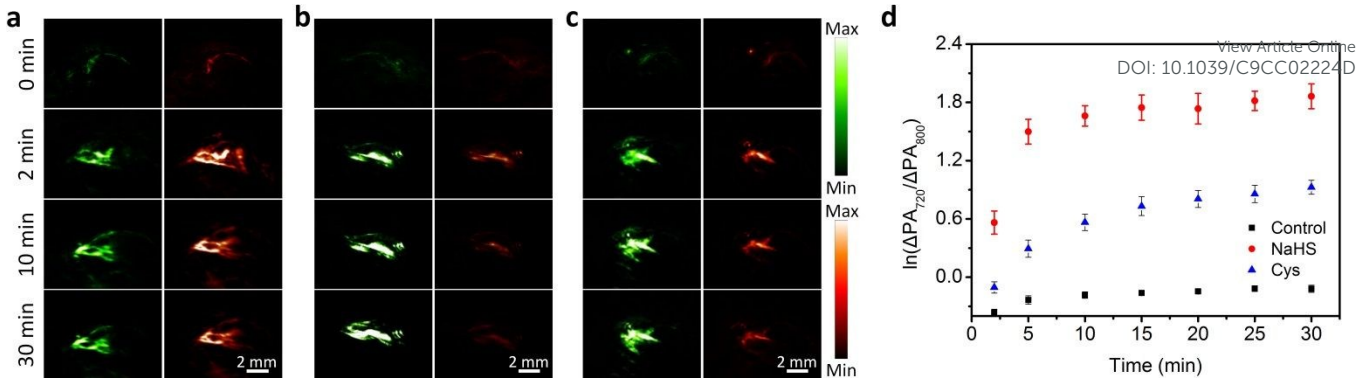


**Fig. 3** *In vivo* PA images of saline (a), NaHS (b) and Cys (c) pretreated regions in the thigh of living mice before (0 min) and after injection of CyCl-1 for 2, 10 and 30 min. The images were presented with pseudo-colors of green for excitation at 720 nm and red for 800 nm. (d) The logarithmic value of ΔPA ratio [$\ln(\Delta PA_{720}/\Delta PA_{800})$] as a function of post-injection time.

intensity of the probe in liver reached the maximum at 3 min and then rapidly decreased, with a decrease of 80% within 3 h (Figure S16c). Bio-distribution of the probe was detected in different organs. 30 min after systemic administration, strong fluorescence signals were observed in the liver of mice, which decreased to the same level as other organs at 3h (Figures S16b and d). Moreover, strong fluorescence was detected from the feces of mice after 2.5 h. These data indicated the rapid clearance of CyCl-1 through the hepato-biliary excretion pathway, which is quite similar to ICG.[17]

In conclusion, we developed a small-molecule PA probe (CyCl-1) that exhibited a dual-peak ratiometric PA signal in the NIR region when exposed to $H_2S$. The probe was constructed based on water soluble cyanine dyes through the nucleophilic substitution of $H_2S$ to active chlorine, which led to significant variations in the PA signals of 800 nm (attenuation) and 720 nm (enhancement). Such molecule design endowed the probe with fast response and high selectivity to $H_2S$. The probe could be used for ratiometric PA monitoring of $H_2S$ in living mice, and provided high imaging fidelity and rapid clearance. We believe that the developed small-molecule ratiometric PA probe can facilitate the application of advanced PA imaging technology in $H_2S$ relevant biomedical and clinical studies.

This work was supported by the National Natural Science Foundation of China (21602112, 21674048 and 21574064), 333 project of Jiangsu province (BRA2016379), Primary Research & Development Plan of Jiangsu Province (BE2016770) and the China Postdoctoral Science Foundation (No. 2017M621792).

## Conflicts of interest

There are no conflicts to declare.

## Notes and references

1. (a) R. Wang, *FASEB J.*, 2002, **16**, 1792; (b) H. Peng, Y. Cheng, C. Dai, A. L. King, B. L. Predmore, D. J. Lefer and B. Wang, *Angew. Chem. Int. Ed.*, 2011, **50**, 9672; (c) H. Kimura, *Amino Acids*, 2011, **41**, 113.
2. (a) T. V. Mishanina, M. Libiad and R. Banerjee, *Nat. Chem. Biol.*, 2015, **11**, 457; (b) P. Bindu D, S. Juan I, X. Risheng, V. M Scott, C. Jiyoung Y, S. Adele M and S. Solomon H, *Nature*, 2016, **509**, 96; (c) J. L. Greaney, J. L. Kutz, S. W. Shank, S. Jandu, L. Santhanam and L. M. Alexander, *Hypertension*, 2017, **69**, 902.
3. (a) W. Min, Z. Jun, P. Yang, D. Jingde, Z. Lili, Z. Xiangrong and Z. Li, *J. Neurosci. Res.*, 2015, **93**, 487; (b) E. Barone, E. Head, D. A. Butterfield and M. Perluigi, *Free Radical Biol. Med.*, 2016, **111**, S0891584916309972; (c) M. M. Safar and R. M. Abdelsalam, *Pharmacol. Rep.*, 2015, **67**, 17.
4. (a) D. Sajal Kumar, L. C. Su, Y. S. Young, H. J. Hee and C. Bong Rae, *Cheminform*, 2012, **48**, 8395; (b) Q. Wan, Y. Song, Z. Li, X. Gao and H. Ma, *Chem. Commun.*, 2013, **49**, 502.
5. (a) Y. Qian, J. Karpus, O. Kabil, S. Y. Zhang, H. L. Zhu, R. Banerjee, J. Zhao and C. He, *Nat. Commun.*, 2011, **2**, 495; (b) W. Xu, J. Sun, W. Zhang, X. Ma, J. Lv and T. Bo, *Chem. Sci.*, 2013, **4**, 2551.
6. K. Sasakura, K. Hanaoka, N. Shibuya, Y. Mikami, Y. Kimura, T. Komatsu, T. Ueno, T. Terai, H. Kimura and T. Nagano, *J. Am. Chem. Soc.*, 2011, **133**, 18003.
7. (a) C. Zhao, X. Zhang, K. Li, S. Zhu, Z. Guo, L. Zhang, F. Wang, Q. Fei, S. Luo and P. Shi, *J. Am. Chem. Soc.*, 2015, **137**, 8490; (b) X. Li, H. Zhao, Y. Ji, C. Yin, J. Li, Z. Yang, Y. Tang, Q. Zhang, Q. Fan and W. Huang, *ACS Appl. Mater. Interfaces*, 2018, **10**, 39544.
8. (a) L. V. Wang and H. Song, *Science*, 2012, **335**, 1458; (b) Y. Jiang and K. Pu, *Small*, 2017, **13**, 1700710; (c) H. J. Knox and J. Chan, *Acc. Chem. Res.*, 2018, **51**, 2897.
9. (a) X. Hu, F. Lu, L. Chen, Y. Tang, W. Hu, X. Lu, Y. Ji, Z. Yang, W. Zhang and C. Yin, *ACS Appl. Mater. Interfaces*, 2017, **9**, 30458; (b) C. Yin, G. Wen, C. Liu, B. Yang, S. Lin, J. Huang, P. Zhao, S. H. D. Wong, K. Zhang, X. Chen, G. Li, X. Jiang, J. Huang, K. Pu, L. Wang and L. Bian, *Acs Nano*, 2018, **12**, 12201; (c) Q. Chen, C. Liang, X. Sun, J. Chen, Z. Yang, H. Zhao, L. Feng and Z. Liu, *Proc. Natl. Acad. Sci. U. S. A.*, 2017, **114**, 5343; (d) Q. Wang, B. Xia, J. Xu, X. Niu, J. Cai, Q. Shen, W. Wang, W. Huang and Q. Fan, *Mater. Chem. Front.*, 2019, DOI: 10.1039/C9QM00036D.
10. (a) J. Zhang, X. Zhen, P. K. Upputuri, M. Pramanik, P. Chen and K. Pu, *Adv. Mater.*, 2017, **29**, 1604764; (b) C. Yin, X. Zhen, Q. Fan, W. Huang and K. Pu, *Acs Nano*, 2017, **11**, 4174; (c) Z. Yang, Y. Dai, C. Yin, Q. Fan, W. Zhang, J. Song, G. Yu, W. Tang, W. Fan and B. C. Yung, *Adv. Mater.*, 2018, **30**, 1707509.
11. Y. Liu, S. Wang, Y. Ma, J. Lin, H. Y. Wang, Y. Gu, X. Chen and P. Huang, *Adv. Mater.*, 2017, **29**, 1606129.
12. C. Yin, Y. Tang, X. Li, Z. Yang, J. Li, X. Li, W. Huang and Q. Fan, *Small*, 2018, **14**, 1703400.
13. (a) Q. Chen, X. Liu, J. Chen, J. Zeng, Z. Cheng and Z. Liu, *Adv. Mater.*, 2016, **27**, 6820; (b) Z. Yang, W. Fan, W. Tang, Z. Shen, Y. Dai, J. Song, Z. Wang, Y. Liu, L. Lin and L. Shan, *Angew. Chem.*, 2018, **130**, 14297; (c) Z. Yang, J. Song, W. Tang, W. Fan, Y. Dai, Z. Shen, L. Lin, S. Cheng, Y. Liu and G. Niu, *Theranostics*, 2019, **9**, 526.
14. B. Shi, X. Gu, F. Qiang and C. Zhao, *Chem. Sci.*, 2017, **8**, 2150.
15. (a) F. Yu, P. Li, P. Song, B. Wang, J. Zhao and K. Han, *Chem. Commun.*, 2012, **48**, 2852; (b) H. Xiao, C. Wu, P. Li, W. Gao, W. Zhang, W. Zhang, L. Tong and B. Tang, *Chem. Sci.*, 2017, **8**, 7025.
16. Z. Yi, C. Wangqiao, Z. Jixin, P. Wenbo, W. Chengyuan, H. Ling, Y. Cheng, Y. Qinyu, H. Wei and J. S. C. Loo, *Small*, 2015, **10**, 4874.
17. H. Shinohara, A. Tanaka, T. Kitai, N. Yanabu, T. Inomoto, S. Satoh, E. Hatano, Y. Yamaoka and K. Hirao, *Hepatology*, 2010, **23**, 137.